Journal of Engineering Science and Technology
Special Issue on ICIT2022 Vol. 19, No. 1 (2024) 25 - 39

NUMERICAL SIMULATION ON THE BEHAVIOR OF CELLULAR STAINLESS-STEEL BEAM (CSSB) AT ELEVATED TEMPERATURE

ADRIAN RUDOLF YANSAI[1], NORLIZAN WAHID[1], LEE HOONG PIN[2], FARIZ ASWAN AHMAD ZAKWAN[1,*], RUQAYYAH ISMAIL[1], GOH LYN DEE[1], HAZRINA AHMAD[1]

[1]Centre for Civil Engineering Studies, Universiti Teknologi MARA, Cawangan Pulau Pinang, Permatang Pauh Campus, 13500 Permatang Pauh, Pulau Pinang, Malaysia
[2]Department of Civil Engineering, Faculty of Engineering and Quantity Surveying, INTI International University, 71800 Negeri Sembilan, Malaysia
Corresponding Author: fariz838@uitm.edu.my

Abstract

Cellular stainless-steel beams (CSSBs) are becoming increasingly popular in building applications due to their superior corrosion resistance and mechanical properties. However, there are no specific design criteria for CSSBs, and it is unclear how different thicknesses of CSSBs behave in the event of a fire. In this research, we investigate the effect of section thickness on the behaviour of CSSBs in a fire and under applied loading. Finite element analysis were performed using ABAQUS CAE software and the model were validated using data from previous experimental studies. From the numerical simulation output, it was revealed that the thinner web thickness of CSSBs fails first at the beginning of fire exposure, while the thicker flange thickness is able to sustain higher strength and stiffness when it fails first during fire exposure and applied loading execution. Additionally, a thicker section of CSSB can dissipate heat uniformly, which is faster than a thinner section. These results highlight the importance of considering section thickness in CSSB design and provide insight into the behaviour of CSSBs in high-temperature environments. It was demonstrated that the compatibility of the current design standards with finite element analysis.

Keywords: Cellular stainless-steel beam (CSSB), Deflection, Elevated temperature, Finite element method (FEM), Fire, Heat transfer analysis, Sustainable and resilient building.

1. Introduction

Stainless steel beams are essential structural elements designed to withstand significant loads in construction and engineering applications. These beams are commonly used in projects requiring strength and corrosion resistance, including buildings, bridges, and other structures [1-5]. H-beams, I-beams, and U-channels are some of the shapes and diameters of stainless steel beams available. Austenitic stainless steel is the most widely used type of stainless steel for beams due to its strength and corrosion resistance. In harsh conditions like coastal areas, chemical facilities, and other corrosive environments, stainless steel beams are preferred over ordinary steel beams because of their superior corrosion resistance. Additionally, stainless steel beams offer a modern and stylish appearance that can enhance the look of a building or structure.

Stainless steel has become increasingly popular as a versatile structural material for load-bearing building applications. It's available in various grades, grouped into five families based on their metallurgical composition: austenitic, ferritic, duplex, martensitic, and precipitation hardened grades [6]. The most commonly used grades for structural applications are austenitic and duplex, which contain 17-18% and 22-23% chromium, respectively [6, 7]. In addition to its corrosion resistance, stainless steel has been found to offer several other advantages, including excellent mechanical properties, low maintenance requirements, long lifespan, good formability, and full recyclability [6, 7].

To ensure corrosion resistance, stainless steel must have a chromium (Cr) content of at least 10.5 percent. Other alloying elements such as carbon (C), nickel (Ni), manganese (Mn), molybdenum (Mo), copper (Cu), silicon (Si), sulphur (S), phosphorus (P), and nitrogen (N) are also present, with the standard code specifying the chemical compositions for various grades. Austenitic and duplex grades are the most common stainless-steel grades used in structural engineering, with austenitic grades having a chromium content of 17-18% and a nickel content of 8-11%, providing excellent corrosion resistance [1-5]. Duplex grades, with a mixed austenitic-ferritic microstructure, have a higher chromium content of 22-23% and nickel content of 4-5%, making them more durable, wear-resistant, and corrosion-resistant than austenitic steels. In civil engineering, EN 1.4301, EN 1.4401, and EN 1.4462 are the most commonly used austenitic and duplex grades [8]. The material properties and selection criteria for these stainless steels have been thoroughly researched [8].

In recent years, there has been growing interest in the behaviour of stainless steel beams in fire conditions. Studies have shown that the web-post temperature of cellular steel beams increases more rapidly than in solid steel beams, which can result in a greater need for passive fire protection. This has been identified as a significant drawback in applications that require extended fire resistance [6, 9]. However, replacing solid carbon steel beams with stainless steel beams can provide a reliable solution for enhancing performance during fire exposure without requiring passive fire protection. This approach can also result in cost savings and faster construction times [6].

The use of cellular stainless-steel beams (CSSBs) is a promising structural solution for long-spanning members, given their superior properties such as corrosion resistance, long service life, excellent mechanical characteristics, formability, recyclability, and low maintenance requirements [6-10]. However, despite the

benefits of using stainless steel in the fabrication of CSSBs, there is a lack of understanding of their behaviour at elevated temperatures. Under the ISO 834 standard fire test, a significant temperature gradient occurs along the height of steel beams with three sides exposed to fire, and the critical temperature of steel members increases as the section factor increases [11].

The literature contains limited fire experiments on structural stainless steel flexural members, as evidenced by a few studies [6, 11, 12]. Stainless steel, in terms of mechanical and physical properties, has been shown to outperform carbon steel in terms of fire behaviour [6, 13]. Structural stainless steel members exposed to fire have higher emissivity and convective heat transfer coefficients than carbon steel members [6, 14]. However, no experiments on stainless steel cellular beams have been reported in the literature to date [6].

2. Methodology

This chapter details the methodology employed in the study, which aims to validate the finite element modelling of CSSB at higher temperatures based on previous experimental work [15, 16]. Additionally, the study aims to investigate the effects of varying web and flange thicknesses on the behaviour of CSSB at elevated temperatures using the ISO834 standard fire curve through parametric research. To accomplish these goals, Finite Element Modelling (FEM) was conducted using ABAQUS CAE software, resulting in four models of CSSB with different thicknesses. The first model was used to validate the CSSB model with previous experimental laboratory data, while the second through fourth models were utilized for parametric analysis. The CSSB design conforms to the austenitic stainless steel beam grade 1.4301, and Table 1 [15, 16], provides detailed dimensions. The yield strength of 1.4301 stainless steel ranges from 210 to 300 MPa, while the ultimate tensile strength varies between 520 and 700 MPa [11, 17], depending on the steel's specific conditions such as temperature and strain rate. Figure 1 depicts the CSSB geometry, while Fig. 2 displays the modelled CSSB from a top section view.

Table 1. The detailed dimension of the CSSB [15, 16].

Stainless steel grade	Length (mm)	Depth (mm)	Width (mm)	Diameter (mm)		
				Circular opening	Web section	Flange section
1.4301	4000	290	300	200	8	14

In terms of the boundary conditions, a pinned support was assumed for both ends of the CSSB model, as illustrated in Fig. 3. To simulate real-world conditions, the beam was subjected to a static load equal to 30% of the design load prior to being placed in the furnace. The fire loading was then carried out in accordance with the ISO834 standard fire curve (Fig. 4) until failure, consistent with previous experimental work [16]. The CSSB was tested under four-point bending conditions with two concentrated applied loads, resulting in consistent bending moments between the loads. The concentrated loads were allocated based on the previous experiment work, with a value of 6.409 kN. To evaluate the FEM of the CSSB at high temperatures, various thicknesses of web and flange sections were created.

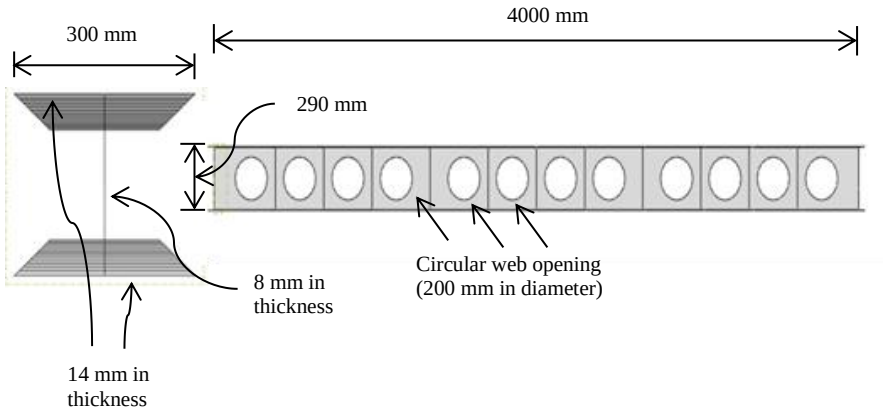

Fig. 1. Front view geometry of the CSSB model.

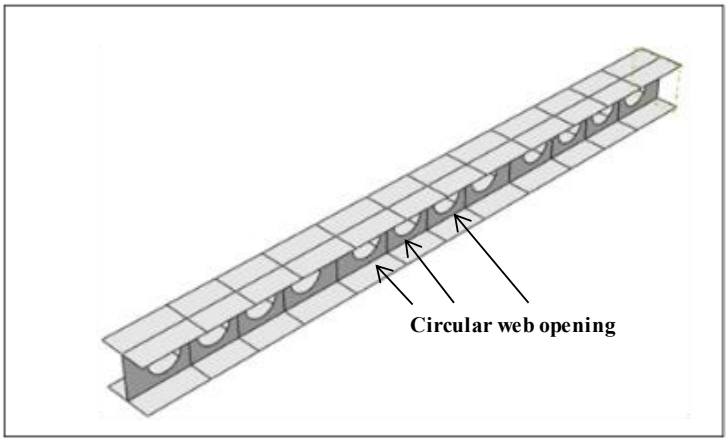

Fig. 2. Image of the CSSB model viewed from top section.

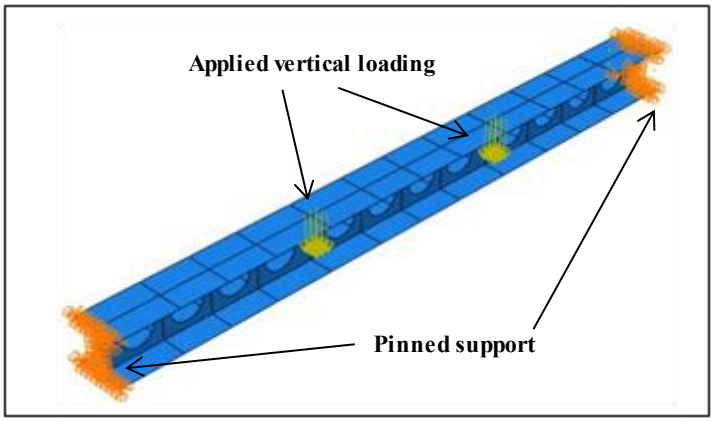

Fig. 3. Boundary condition location at both end of the CSSB model and applied loading location on top of the CSSB model.

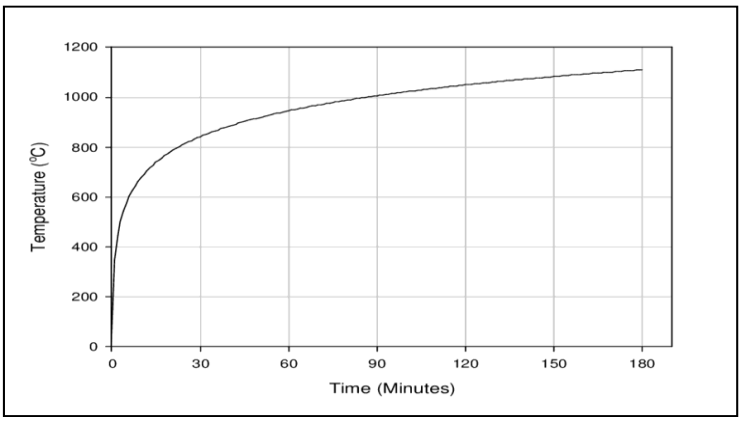

Fig. 4. ISO 834 standard fire curve.

2.1. Material properties of the CSSB

While the study utilized material parameters from earlier research work [18, 19] for heat transfer and static loading analysis, it should be noted that due to the lack of material characteristics information for stainless steel beams, only normal steel beam material properties were assumed. The ISO834 standard fire curve was used to simulate the actual fire exposure, with a heat transfer analysis duration of 20 minutes (1200 seconds) corresponding to the experimental data. To model the interaction between the fire exposure and CSSB surface, surface film condition and surface radiation were employed. The surface film condition had a value of 25 W/m2 K for heating and 9 W/m2 K for cooling, with the ISO834 fire curve using sink temperature to connect this relationship. The study also considered surface radiation, which describes heat transmission in a nonconvex environment, using a cavity approximation with a uniform emissivity distribution and an ambient temperature of 0.825. Finally, in the experiment, heat was applied to the bottom and sides of the CSSB, while the top surface of the top flange was covered with aerated concrete block.

2.2. Heat transfer analysis

It is commonly known that the temperature in a fire increases and fluctuates over time. In response to heat transfer, the surface of the CSSB must interact with the heat. In this research work, the fire was applied to the bottom and sides of the beam, while the top was covered by an aerated concrete block serving as a slab. The amplitude of the model was determined based on a tabular amplitude from the ISO834 Standard Fire Curve (BS EN 1991-1-2) [20].

Heat transfer analysis can be divided into two main components: convection, which involves the transfer of heat through a fluid or gas, and radiation, which involves the transfer of heat through electromagnetic waves. These processes occur across the boundary from fire exposure, as well as within the structural elements themselves through conduction. When a structural member is exposed to fire, it experiences heat transfer from both convection and radiation. After the early stage of the fire, radiation becomes much more dominant than convection. The surface

of the structural element is subject to thermal actions that can be represented by a net heat flux, $\dot{h}_{net}$. A net heat flux, $\dot{h}_{net}$ is imposed on the bare surface of structural elements as follows:

$$\dot{\mathrm{h}}_{\mathrm{net}} = \dot{\mathrm{h}}_{\mathrm{net,c}} + \dot{\mathrm{h}}_{\mathrm{net,r}} \qquad (\mathrm{W/m^2}) \qquad (1)$$

The net convective heat flux, $\dot{h}_{net,c}$ can be calculated as follows:

$$\dot{h}_{net,c} = \alpha_c \cdot \left(\Theta_g - \Theta_m\right) \qquad (\mathrm{W/m^2}) \qquad (2)$$

where, α_c= the coefficient of heat transfer by convection ($\mathrm{W}/m^2\mathrm{K}$), Θ_g= the gas temperature near the fire exposed member (°C) and Θ_m= the surface temperature of the member (°C). The value of the coefficient of heat transfer by convection, α_c can be retrieved from Table 2 as follows:

Table 2. The coefficient of heat transfer by convection as in BS EN 1991-1-2 [20].

Fire model or exposed condition	$\boldsymbol{\alpha_c}$ $\mathbf{(W/m^2K)}$
Standard fires	25
External fires	25
Hydrocarbon fires	50
Parametric fires	35
Unexposed side of separating members without radiation	4
Unexposed side of separating members with radiation	25

The net radiative heat flux, $\dot{h}_{net,r}$ is approximately obtained from BS EN 1991-1-2 [20] as follows:

$$\dot{h}_{net,r} = \Phi \cdot \varepsilon_m \cdot \varepsilon_f \cdot \sigma \cdot [(\Theta_r + 273)^4 - (\Theta_m + 273)^4] \quad [\mathrm{W/m^2}] \qquad (2)$$

where, Φ= the configuration factor, ε_m= the surface emissivity of the member, ε_f= the emissivity of the fire, σ= the Stephan Boltzmann constant ($= 5.67x10^{-8}$ $\mathrm{W}/m^2\mathrm{K}^4$), Θ_r= the effective radiation temperature of the fire environment (°C) and Θ_m= the surface temperature of the member (°C). Generally, the emissivity of the fire, ε_f and the configuration factor, Φ is taken as 1.0. The configuration factor, Φ are solely depends on two effects, namely position effect and shadow effect. The surface emissivity of the member, ε_m can be taken from Table 3 as follows:

Table 3. Emissivity of materials.

Material	**The surface emissivity of the member, $\boldsymbol{\varepsilon_m}$**
Carbon steel [21]	0.7
Stainless steel [21]	0.4
Concrete [22]	0.7
Others [20]	0.8

The thermal elongations for both structural carbon steel and reinforcing steels, $\Delta\, l/l$ can be taken equally as in design codes of BS EN 1993-1-2 and BS EN 1994-1-2 [21, 22]. The thermal elongation against temperature modification of steel and reinforcing steel were taken from available codes [21, 22]. The specific heat against

temperature modification of steel and reinforcing steel were also taken from available codes [21, 22]. The thermal conductivity against temperature modification of steel and reinforcing steel were taken from available codes [21, 23].

2.3. Finite element method (FEM) modelling

The CSSB was modelled using the finite element analysis software ABAQUS CAE, with shell elements (specifically, S4R elements from the ABAQUS library) used to mimic the behaviour of the board, as shown in Fig. 5 [6, 10]. This approach is suitable for thin shell applications, and each corner node of the model has six degrees of freedom. To ensure accurate results while maintaining computational efficiency, mesh convergence research was conducted to determine the appropriate mesh density. The finite element analysis of the CSSB is conducted in two stages. First, a mechanical load is applied to the model. This load is then maintained while elevated temperature output is applied to the CSSB in the second stage of the analysis.

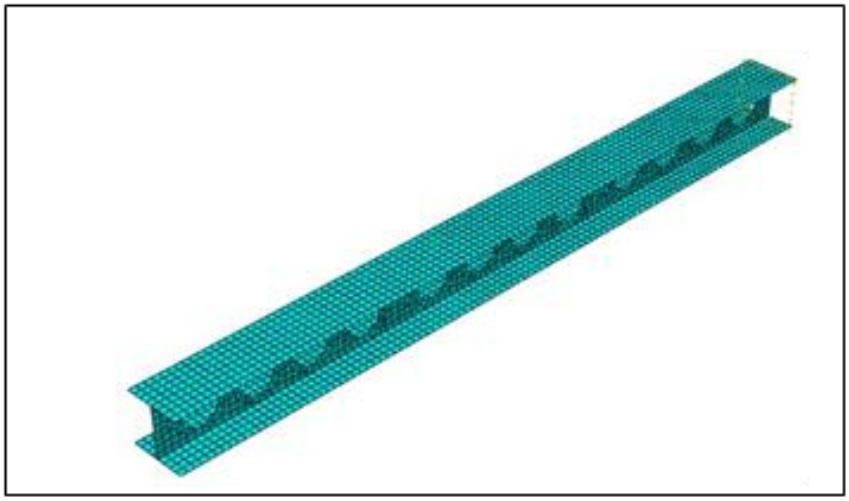

Fig. 5. Meshing procedure output of the CSSB model.

2.4. Parametric investigations on the CSSB

This model consists of two stages, where the first stage involves gathering temperature output data during heat transfer analysis. However, during fire exposure, the temperature doesn't remain constant but increases with time. Therefore, to understand the structure's behaviour at elevated temperatures, parametric studies are needed through multiple analyses. To fulfil the third objective of this study, we constructed a static mechanical model and incorporated the results of the heat transfer analysis into it. We loaded the temperature output database (ODB) file into the ABAQUS program using the predefined fields sub-options. The CSSB model presented in Fig. 2 is identical to our model. To achieve the final goal of this research, we developed four models - one to simulate load analysis and three to replicate the load analysis model's output.

3. Results and Discussion

3.1. Validation of finite element analysis (FEA)

In this paper, we employed a finite element model that was validated using experimental work conducted by previous researchers [15, 16]. To ensure the accuracy of the validation process, we selected three locations along the flange and web section of the CSSB model - node no. 41, 43, and 33, as depicted in Fig. 6. The validation results between the experimental work and finite element analysis for the predicted CSSB are shown in Figs. 7, 8, and 9. It can be observed that the discrepancies between the numerical and experimental results are minimal. We also displayed the temperature variations at the end of the fire exposure in Table 4, which correspond to node 33, 43, and 41, respectively. Node 33 shows a 2.13% difference from the experimental data, while nodes 41 and 43 both exhibit a 1% difference.

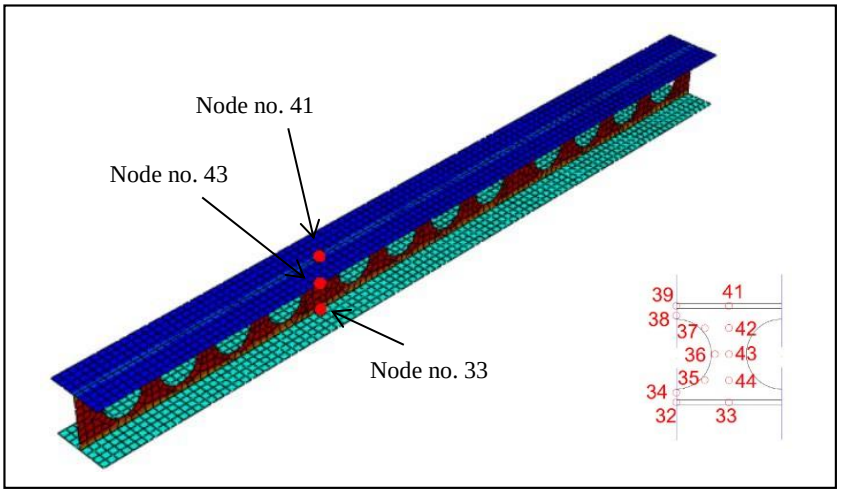

Fig. 6. Location node 41, 43 and 33 of the CSSB model.

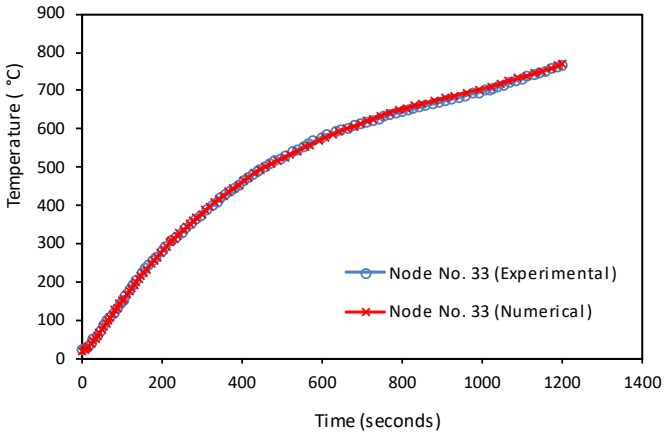

Fig. 7. Maximum predicted temperature vs. time of node no. 41 of the CSSB model.

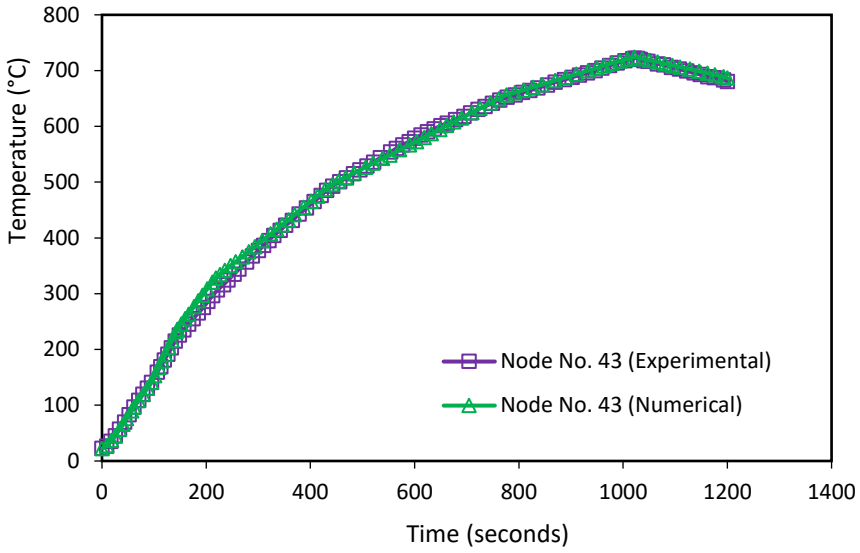

Fig. 8. Maximum predicted temperature vs. time of node no. 43 of the CSSB model.

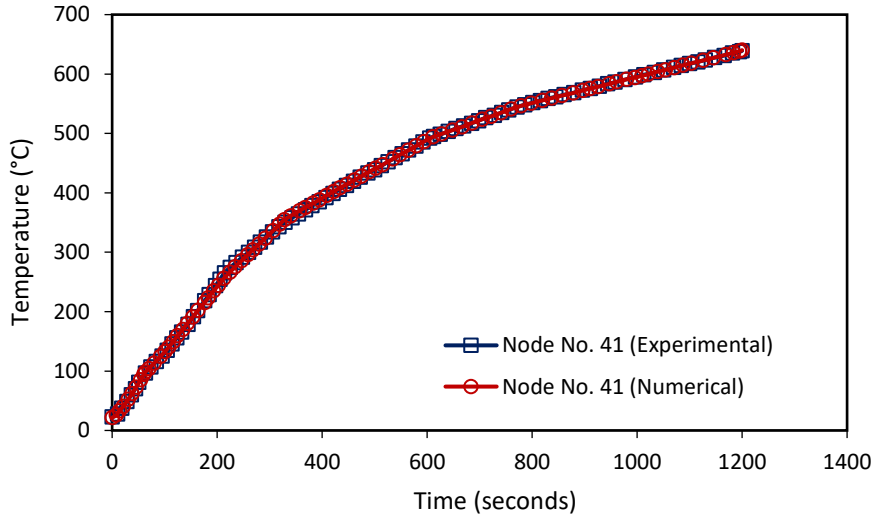

Fig. 9. Maximum predicted temperature vs. time of node no. 33 of the CSSB model.

Table 4. Maximum predicted temperature between the experimental and numerical analysis.

Node No.	Maximum temperature (°C)		
	33	**43**	**41**
Experimental	752	681	639
Numerical	768	686	641
Error (%)	2.13	1.0	1.0

3.2. Heat transfer analysis results

The heat transfer study yielded the thermal behaviour distribution for all three CSSB models. We measured the nodal temperatures (NT11) of the beam for each model, which were used to represent the temperature behaviour at various locations along the CSSB model in the ABAQUS FE modelling. Figs. 10 and 11 depict the predicted temperature output for various web and flange thicknesses.

We considered web thicknesses of 6, 10, and 12 mm, and flange thicknesses of 12, 16, and 18 mm for the three parametric models - Model 1 (M1), Model 2 (M2), and Model 3 (M3), respectively. All the variations in web and flange thicknesses are presented in Table 5. The results indicate that the anticipated temperature along the web and flange sections of the model was lower than the normal ISO 834 fire curve, as shown in Fig. 10.

However, M1, with a web thickness of 6 mm and flange thickness of 12 mm, had the largest anticipated temperature distribution and quickly surged over the ISO834 fire curve during the thermal distribution after being subjected to fire for approximately 1000 seconds. This could be due to the material thickness being unable to withstand the high temperature exposure. Nevertheless, the heat dispersion along the CSSB model is much lower than that of the web portion, especially in the flange area.

The maximum heat distribution was predicted at the web sections during CSSB simulation at increased temperatures, whereas reduced heat distribution was projected at the flange section. Table 5 shows the thickness of the web and flange sections for each CSSB model, while Table 6 shows the highest anticipated temperature for each model at the conclusion of the fire exposure.

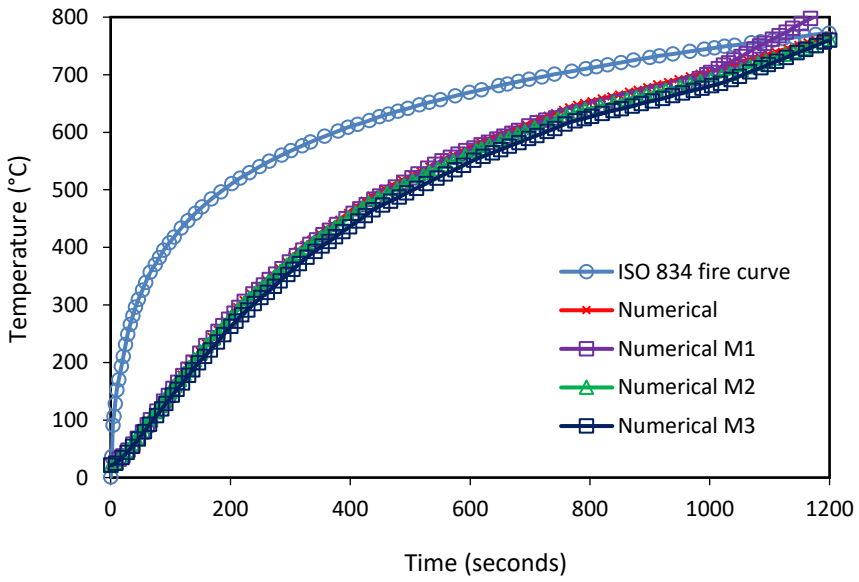

Fig. 10. Predicted maximum temperature along web section of the CSSB model against time.

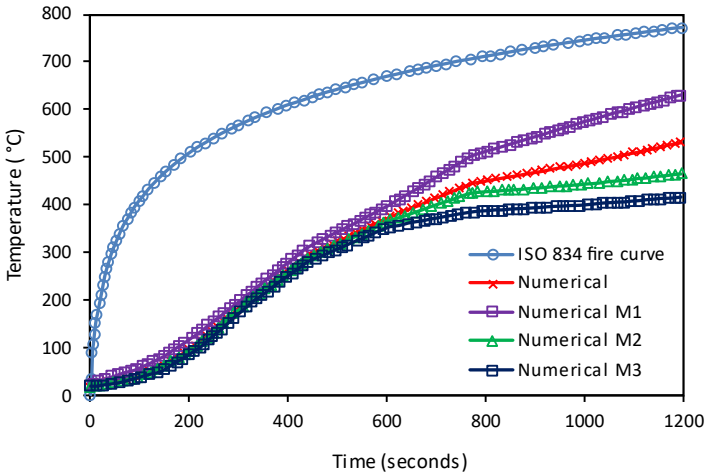

Fig. 11. Predicted maximum temperature along flange section of the CSSB model against time.

Table 5. Variation of web and flange thickness of the CSSB model.

Model	Thickness (mm)	
	Web Section	Flange section
Numerical model	8	14
Model 1 (M1)	6	12
Model 2 (M2)	10	16
Model 3 (M3)	12	18

Table 6. Maximum temperature prediction for each model's section.

Model	Temperature (°C)		
	ISO 834	Web section	Flange section
Numerical model	-	768	533.516
Model 1 (M1)	772	817	631.031
Model 2 (M2)	772	762	465.808
Model 3 (M3)	772	761	415.534

3.3. Stress vs strain behaviour

In this chapter, the stress-strain behaviour of the CSSB model under the influence of heat and axial movement was thoroughly investigated. The stress-strain curves for both web and flange sections of the CSSB models are depicted in Figs. 12 and 13, respectively. During the fire exposure, parametric analysis of the stress-strain relationship was conducted. Node no. 33 was selected for the flange section of the CSSB, while node no. 43 was chosen for the web section, as shown in Fig. 6. The model with an 8 mm web section thickness (M1) exhibited the highest measured stress value, with a strain of 0.01699 mm and a value of 4.6097 MPa. On the other hand, the model with a web thickness of 12 mm (M3) had the lowest stress value. Table 7 presents the predicted maximum yield strength for all CSSB models. As the web thickness is reduced, the stress increases. The ultimate strength of the CSSB is significantly reduced after being exposed to fire, indicating that fire has a substantial impact on the CSSB's structural integrity.

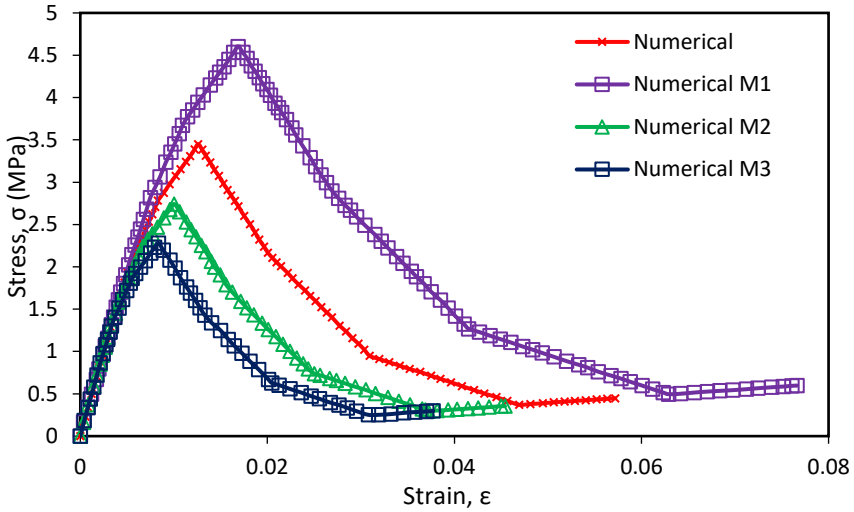

Fig. 12. Predicted stress vs strain relationship along the web section of the CSSB model.

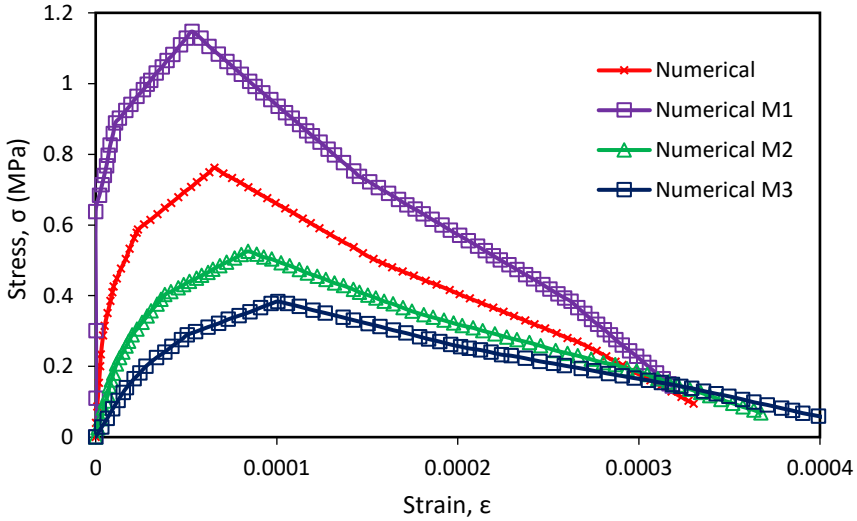

Fig. 13. Predicted stress vs. strain relationship along the web section of the CSSB model.

Table 7. Predicted maximum yield strength of the CSSB model between experimental and numerical analysis.

Model	Maximum Yield Strength (MPa)	
	Web Section	Flange section
Numerical model	3.44944	0.76094
Model 1 (M1)	4.6097	1.14701
Model 2 (M2)	2.75101	0.52601
Model 3 (M3)	2.2845	0.38366

4. Conclusions

In conclusion, this study presents a useful finite element model to investigate the behaviour of a CSSB under elevated temperature loading. The model was validated against experimental data and proven to be accurate in predicting the temperature distribution, stress-strain relationship, and yield strength of the beam. The study also examines the effect of different thicknesses on the beam's behaviour under high-temperature conditions. This work provides a foundation for future studies to investigate the impact of other factors on the behaviour of the CSSB, which will improve the understanding of these structural elements and contribute to the development of realistic design suggestions. Overall, this study provides valuable insights into the behaviour of CSSBs under severe conditions and can be a valuable resource for engineers and researchers working in this field.

Acknowledgment

The authors would like to thank to the Civil Engineering Studies, College of Engineering, Universiti Teknologi MARA, Cawangan Pulau Pinang, Permatang Pauh Campus, Permatang Pauh, Pulau Pinang, and School of Civil Engineering, College of Engineering, Universiti Teknologi MARA, Shah Alam, Selangor who contributed to the experimental data used in this study. Without their support, this research would not have been possible. Finally, the authors would like to acknowledge the valuable insights and suggestions provided by their colleagues and reviewers, which have significantly improved the quality of this work.

Nomenclatures

A	The area across which heat is transferred, m^2
c	The specific heat of the material, J/kg K
c_a	The specific heat of carbon steel and reinforcing steel, J/kg K
$\dot{h}_{net}$	Net heat flux
$\dot{h}_{net,c}$	Net convective heat flux
$\dot{h}_{net,r}$	The net radiative heat flux
k	The thermal conductivity of the material, W/m K
l	The length at 20°C of the steel member, m
P	the density of the material, kg/m^3
Q	The internal energy generated within the element, W/m^3
q	The heat transfer rate across the area A, W
T	Temperature, K
t	Time, s
X	The distance normal to the area A, m

Greek Symbols

α_c	The coefficient of heat transfer by convection (W/m^2K)
Δl	The temperature which generates elongation of the steel member
$\Delta l/l$	The thermal elongations
ε_f	The emissivity of the fire
ε_m	The surface emissivity of the member
θ_a	The steel temperature, °C
Θ_g	The gas temperature near the fire exposed member, °C
Θ_m	The surface temperature of the member, °C
Θ_r	The effective radiation temperature of the fire environment, °C

λ_a	The thermal conductivity of steel, W/m·K
σ	The Stephan Boltzmann constant ($= 5.67x10^{-8}$ W/m^{2}K^4)
Φ	The configuration factor

Abbreviations

CAE	Computer-aided engineering
CSSB	Cellular stainless-steel beam
FE	Finite element
FEA	Finite element analysis
FEM	Finite element method
ODB	Output database
SSB	Stainless-steel beam

References

1. Fan, S.; Du, L.; Li, S.; Zhang, L.; and Shi, K. (2019). Fire-resistance of RHS stainless steel beams with three faces exposed to fire. *Journal of Constructional Steel Research*, 152, 284-295.
2. Khan, M.A.; Khan, A.A.; Cashell, K.A.; and Usmani, A. (2022). Response of restrained stainless steel corrugated web beams at elevated temperature. *Structures*, 41, 668-683.
3. Wu, M.; Fan, S.; Zhou, H.; Han, Y.; and Liang, D. (2022). Experimental and numerical research on fire resistance of stainless steel-concrete composite beam. *Journal of Constructional Steel Research*, 194, 107342.
4. Lopes, N.; Couto, C.; Real, P.V.; Camotim, D.; and Gonçalves, R. (2022). Fire design of stainless steel I beams prone to lateral torsional buckling under end moments. *Fire Safety Journal*, 131, 103609.
5. Ding, R.; Fan, S.; Wu, M.; and Li, Y. (2021). Numerical study on fire resistance of rectangular section stainless steel-concrete composite beam. *Fire Safety Journal*, 125, 103436.
6. Cashell, K.A.; Malaska, M.; Khan, M.; Alanen, M.; and Mela, K. (2021). Experimental and numerical analysis of stainless steel cellular beams in fire. *Fire Safety Journal*, 121, 103277.
7. Afshan, S.; Arrayago, I.; Gardner, L.; Gedge, G.; Jandera, M.; Ral, E.; Rossi, B.; Stranghöner, N.; and Zhao, O. (2017). *Design manual for structural stainless steel*. (4th ed.). Steel Construction Institute publications.
8. Gardner, L. (2005). The use of stainless steel in structures. *Progress in Structural Engineering and Materials*, 7(2), 45-55.
9. Mesquita, L.; Gonçalves, J.; Gonçalves, G.; Piloto, P.; and Abdelhak, K. (2015). Intumescente fire protection of cellular beams. *X Congresso de Construção Metálica e Mista*, 623-630.
10. Chen, Z.; Huang, Y.; and Young, B. (2022). Design of cold-formed ferritic stainless steel RHS perforated beams. *Engineering Structures*, 250, 113372.
11. Li, S.; Ding, W.; Zhang, Q.; Xiao, X.; and Zhou, Q. (2022). Experimental study of the mechanical properties of a new duplex stainless steel exposed to elevated temperatures. *Case Studies in Construction Materials*, 17, e01683.

12. Fan, S.; Jia, L.; Lyu, X.; Sun, W.; Chen, M.; and Zheng, J. (2017). Experimental investigation of austenitic stainless steel material at elevated temperatures. *Construction and Building Materials*, 155, 267-285.
13. Gardner, L.; and Baddoo, N.R. (2006). Fire testing and design of stainless steel structures. *Journal of Constructional Steel Research*, 62(6), 532-543.
14. Gardner, L.; and Ng, K.T. (2006). Temperature development in structural stainless steel sections exposed to fire. *Fire Safety Journal*, 41(3), 185-203.
15. Gardner, L.; and Ng, K.T. (2006). Temperature development in structural stainless steel sections exposed to fire. *Fire Safety Journal*, 41(3), 185-203.
16. Molkens, T.; Cashell, K.A.; Malaska, M.; Alanen, M.; and Rossi, B. (2021). Post-fire behaviour of structural stainless steel. *ce/papers*, 4(2-4), 1411-1420.
17. Ao, S.; Cheng, M.P. ; Zhang, W. ; Oliveira, J.P.; Manladan, S.M.; Zeng, Z.; and Luo, Z. (2022). Microstructure and mechanical properties of dissimilar NiTi and 304 stainless steel joints produced by ultrasonic welding. *Ultrasonics*, 121, 106684.
18. Nadjai, A.; Vassart, O.; Ali, F.; Talamona, D.; Allam, A.; and Hawes, M. (2007). Performance of cellular composite floor beams at elevated temperatures. *Fire Safety Journal*, 42(6-7), 489-497.
19. Nadjai, A.; Goodfellow, N.; Talamona, D.; Ali, F.; Bailey, C.G.; and Siamak, B.M. (2007). Experimental and numerical investigation on composite floor cellular steel beams in fire. *Proceedings of the* 3*rd International Conference on Steel and Composite Structures* (*ICSCS*07). Manchester, UK, 673-679.
20. BSI (2002) BS EN 1991-1-2:2002 Actions on structures - Part 1-2: General actions - Actions on structures exposed to fire.
21. 2BSI (2005) BS EN 1993-1-2:2005 Design of steel structures - Part 1-2: General rules - Structural fire design.
22. BSI (2005) BS EN 1994-1-2:2005 Design of composite steel and concrete structures - Part 1-2: General rules - Structural fire design.
23. Leong, W.Y. (2023). Digital technology for ASEAN energy. *Proceedings of the* 2023 *International Conference on Circuit Power and Computing Technologies* (*ICCPCT*), Kollam, India, 1480-1486.